SPACE DEBRIS ATMOSPHERIC ENTRY PREDICTION WITH SPACECRAFT-ORIENTED TOOLS

J. Annaloro(1), S. Galera(1,2), P. Kärräng(3), Y. Prévereaud(4),

J-L. Vérant(4), M. Spel(5), P. Van Hauwaert(6), P. Omaly(1)

(1)*CNES Toulouse, 18 avenue Edouard Belin, 31400 Toulouse FRANCE, Email: julien.annaloro@cnes.fr*
(2) *ALTRAN SO, 4 avenue Didier Daurat, 31700 Blagnac, FRANCE*
(3) *HTG, Albert-Einstein-Straße 1137191 Katlenburg-Lindau, GERMANY*
(4) *ONERA Toulouse Center, 2 avenue Edouard Belin, 31055 Toulouse, FRANCE*
(5) *R.Tech, Parc Technologique Delta Sud, 09340 Verniolle, FRANCE*
(6) *R.Tech, Eekholt 42, 1112XH Diemen, THE NETHERLANDS*

Proc. 7th European Conference on Space Debris, Darmstadt, Germany, 18–21 April 2017, published by the ESA Space Debris Office
Ed. T. Flohrer & F. Schmitz, (http://spacedebris2017.sdo.esoc.esa.int, June 2017)

ABSTRACT

This paper deals with the comparison between high-fidelity codes:

- DSMC computations from the Dogra's paper,
- CFD computations from MISTRAL, LORE and CELHYO,

And spacecraft-oriented tools, used to predict the survivability of space debris during the re-entries and assess the prospective risk on ground:

- PAMPERO,
- SCARAB,
- FAST/MUSIC.

Three test-cases have been identified in order to highlight the physical phenomena still to be improved for this type of codes. This paper is in the continuity of the preliminary works from the Ref. [1].

1 INTRODUCTION

In the frame of the French Space Operation Act (LOS) signed on 3rd June 2008, CNES is particularly interested by re-entries of space debris. CNES is indeed in charge of ensuring the right application of the law, notably through the use of DEBRISK [2], for every mission launched or operated from the French territory. To predict the debris survivability during their re-entries and assess the prospective risk on ground, the development of complete multidisciplinary tools is required.

At present, these aerothermodynamics tools can be classified into two categories: the object-oriented tools and the spacecraft-oriented tools. This communication is in the framework of the second category of tools.

Usually, this kind of engineering codes exhibit results with a good agreement obtained for blunt body but some discrepancies can be observed

- For particular shapes where the classical aerothermodynamics models applied to these tools are not appropriate (e.g. flat surface, concave surface),
- For regions influenced by a more complex flow such as shock-boundary layer interaction or elliptic flow regions.

First we propose a brief overview of the codes most often used in this paper, performing the computation of the test-cases below: PAMPERO [3], SCARAB [4], FAST/MUSIC [5] and MISTRAL [6]

Secondly, test cases will be identified aiming at comparing for simple geometries the behavior of the fragments generated at the break-up altitude from a satellite reentering into the atmosphere, or resulting from launch failure problem. In a second phase, we will focus our attention on the reentry of more complex geometry objects corresponding to space vehicles like ARD & PRE-X. The test cases were chosen in order to highlight that these models currently implemented into spacecraft-oriented tools, require notable improvements for specific situations and / or geometries.

Finally, the given results will be analyzed by comparison with CFD/DSMC data regarding aerothermodynamics coefficients. The limits of the approach used in spacecraft-oriented tools will be discussed, paving the way for future developments.

2 TOOLS PRESENTATION

2.1 PAMPERO

PAMPERO is a CNES spacecraft-oriented tool developed since 2013.

The trajectory and the attitude of the object (6 DOF) are integrated with the classical Runge-Kutta method. Local pressure and friction coefficients can be calculated for the three regimes (i.e free molecular, transitional and continuum). Stagnation point convective heat flux is estimated by analytical formulas where correlations are derived from CFD/DSMC computations. An empirical function, depending on the curvature radius and local pressure, is used for the convective heat flux computation all around the object. Bridging functions are necessary to deal with the transitional regime. Radiative heat fluxes losses from the wall object are also computed. No radiation is taken into account from the shock layer. A 3D thermal module is used to calculate diffusion heat fluxes on the surface and inside the object. An ablation module has been also implemented in PAMPERO.

PAMPERO is currently in an important validation phase where a large number of comparisons are being performed, with experiments, CFD/DSMC computations and other spacecraft-oriented tools.

2.2 SCARAB

SCARAB (Spacecraft Atmospheric Re-Entry and Aerothermal Break-Up) is a spacecraft-oriented software tool allowing the analysis of mechanical and thermal destruction of spacecraft and other objects during re-entry. It is an integrated software package (six degrees-of-freedom flight dynamics, aerodynamics, aerothermodynamics, thermal- and structural analysis) used to perform re-entry risk assessments (quantification, characterization and monitoring of surviving fragments during re-entry). The software application has been validated with in-flight measurements, re-entry observations and wind tunnel experiments, and it has been compared to other re-entry prediction tools of the international community.

SCARAB has been developed under ESA/ESOC contracts since 1995 under the lead of HTG (Hypersonic Technology Göttingen) and with support from other European and international partners. It is considered as operational software. The software development has evolved over time, based on lessons learned from preceding software versions, upgrades and specific re-entry analyses performed for various satellites (e.g. ROSAT, BeppoSAX, TerraSAR-X, GOCE, Sentinel-1/2/3/5P/6, SWARM, Cluster-II, Integral, EnMap, EarthCARE), and for the ATV and the ESA launcher programs. Typical launch vehicle (or similar) re-entry applications have been: Ariane-5 stages (EPC, EPS/VEB, ESC-A), Vega stages (Zefiro-9, AVUM), and ATV. SCARAB version 3.1L has been used for this paper.

2.3 FAST/MUSIC

Since 2006, ONERA has been developing 6 DOF FAST/MUSIC to compute the atmospheric re-entry of controlled (guidance and control) and uncontrolled objects such as space debris, asteroids, and vehicles (multi-objects following is allowed). FAST/MUSIC aims to become a Spacecraft-Oriented Code. This code is the gathering of the GNC (Guidance Navigation Control) code MUSIC (Multi Simulator in Combination) [7] with the aerothermodynamic code FAST (Fast Aerothermodynamic Solver for Trans-atmospheric vehicle). In other words, the software includes flight dynamics, aerodynamics, aerothermodynamics and thermal analysis in order to give aerodynamic force and moment coefficients, heat fluxes (convective, diffusive, radiative and conductive) on and inside the debris, as well as the thermo-structural degradation (oxidation, ablation) of objects along their entry trajectories whatever the flow regime. The trajectory of fragments are obtained by numerical integration of the 3 or 6 degrees of freedom equations of motion by a Runge-Kutta scheme or a fourth order predictor-corrector scheme.

FAST/MUSIC has been compared to experiment, numerical (CFD/DSMC) data but also to other spacecraft-oriented codes for various geometry shapes encountered. The code was intensively used as a pre-design tool in the FP7 project “HYPMOCES” aiming at designing the Cabin Escape System from SPACELINER aircraft [7]

2.4 MISTRAL

The high-fidelity reference code often chosen for this communication is MISTRAL developed by the RTECH company. MISTRAL is a toolbox including different solvers, among which a CFD solver and a DSMC solver. The CFD solver resolves the three dimensional Navier-Stokes or Euler equations, taking into account thermochemical non equilibrium gas compositions including weak ionization. A block structured mesh is used to assure high quality results on a minimum number of cells. The DSMC module uses an automatic meshing scheme both in two and three dimensions. The DSMC grid convergence criterion is satisfied with the automatic grid adaptation. Both tools are parallelized to run on massively parallel machines.

3 TEST-CASES

The proposed test-cases are divided into three parts: the rarefied regime, the continuum regime for simple geometries and the continuum regime for space vehicle.

3.1 The rarefied regime

This part is focused on the rarefied regime over a 1.6-meter-diameter sphere. Results from PAMPERO, SCARAB and FAST/MUSIC are compared to direct simulation Monte Carlo (DSMC) calculations from Dogra *et al.* [8] and MISTRAL (DSMC Solver). The flow conditions considered are representative of re-entries of typical satellites or space vehicles. The altitude range considered encompasses the end of the continuum regime (90 km), the transitional regime (from 100 to 130 km) and the free molecular regime (above 140 km). Free-stream velocity is equal to 7.5 km/s. The wall temperature of the sphere is assumed to be a uniform along the surface and equal to 350 K. Upstream conditions are defined in Table 1.

Altitude [km]	**Density [kg/m^3]**	**Temperature [K]**	**Pressure [Pa]**
90	$3.43\text{x}10^{-6}$	188	$1.8615\text{x}10^{-1}$
100	$5.66\text{x}10^{-7}$	194	$3.2327\text{x}10^{-2}$
110	$9.67\text{x}10^{-8}$	247	$7.2953\text{x}10^{-3}$
120	$2.27\text{x}10^{-8}$	368	$2.6569\text{x}10^{-3}$
130	$8.23\text{x}10^{-9}$	500	$1.3453\text{x}10^{-3}$
140	$3.86\text{x}10^{-9}$	625	$8.0845\text{x}10^{-4}$
160	$1.32\text{x}10^{-9}$	822	$3.7983\text{x}10^{-4}$
200	$3.29\text{x}10^{-10}$	1026	$1.2780\text{x}10^{-4}$

Table 1: Upstream conditions from Dogra et al.

Figure 1 shows results comparison between PAMPERO, SCARAB, FAST/MUSIC and the DSMC calculations from Dogra *et al.* and MISTRAL (DSMC) on the drag coefficient Moreover, discrepancies are also plotted between the spacecraft-oriented tools, MISTRAL and the results from Dogra *et al.*, considered as reference. We notice:

- A very good agreement for SCARAB and MISTRAL for all regimes (max 6.6% at 120 km for SCARAB and max 1.5% at 110 km for MISTRAL),
- For PAMPERO and FAST/MUSIC, the agreement is also very good at 90 km and for the free molecular regime,
- Small discrepancies arise in the transitional regime (max 15% at 110 km for PAMPERO and max 12% at 100 km for FAST/MUSIC).

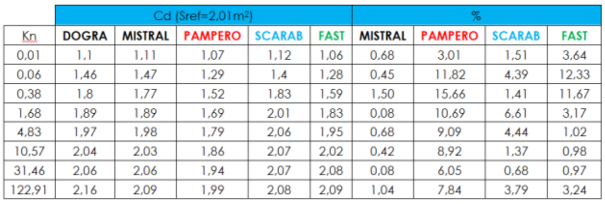

	Cd (Sref=2,01m²)					%			
Kn	DOGRA	MISTRAL	PAMPERO	SCARAB	FAST	MISTRAL	PAMPERO	SCARAB	FAST
0,01	1,1	1,11	1,07	1,12	1,06	0,68	3,01	1,51	3,64
0,06	1,46	1,47	1,29	1,4	1,28	0,45	11,82	4,39	12,33
0,38	1,8	1,77	1,52	1,83	1,59	1,50	15,66	1,41	11,67
1,68	1,89	1,89	1,69	2,01	1,83	0,08	10,69	6,61	3,17
4,83	1,97	1,98	1,79	2,06	1,95	0,68	9,09	4,44	1,02
10,57	2,04	2,03	1,86	2,07	2,02	0,42	8,92	1,37	0,98
31,46	2,06	2,06	1,94	2,07	2,08	0,08	6,05	0,68	0,97
122,91	2,16	2,09	1,99	2,08	2,09	1,04	7,84	3,79	3,24

Figure 1: Drag coefficient versus the Knudsen number

Figure 2 and Figure 3 present respectively the discrepancy between the stagnation pressure from the spacecraft-oriented tools, MISTRAL and the DSMC computation from Dogra *et al.* (reference) and the pressure distribution along the sphere for 3 altitudes: 90, 130 and 200 km. Figure 4 and Figure 5 exhibit respectively the stagnation point heat flux versus the Knudsen number and the heat flux distribution along the sphere for the same altitudes. The computed profiles show that for transition and free molecular altitudes, pressure and heat fluxes distributions are in good overall agreement. Near stagnation point regions:

- Very good agreement for all codes on the stagnation pressure and the pressure distribution (max 7% for PAMPERO, max 7.7% for SCARAB, max 4.4% for FAST/MUSIC and max 4% for MISTRAL)
- For the stagnation heat flux, results for all codes are relatively good except for the transitional regime where discrepancies are noticed (max 41% for PAMPERO at 110 km, max 30% for SCARAB at 100 km, max 16% for FAST/MUSIC at 110 km)

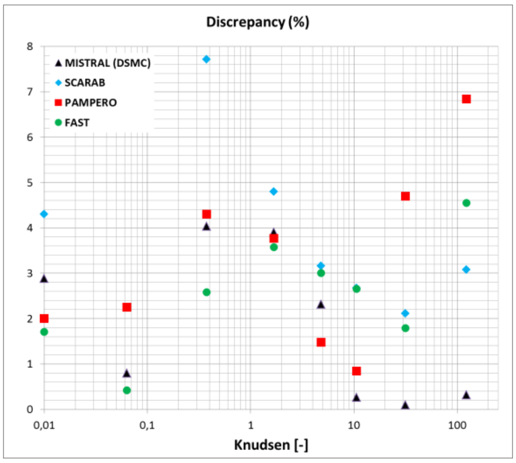

Figure 2: Stagnation pressure versus Knudsen number.

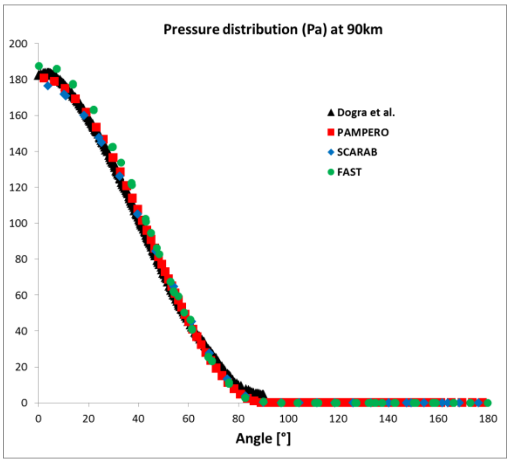

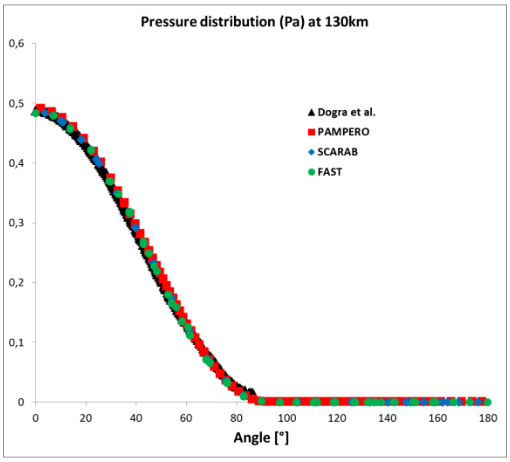

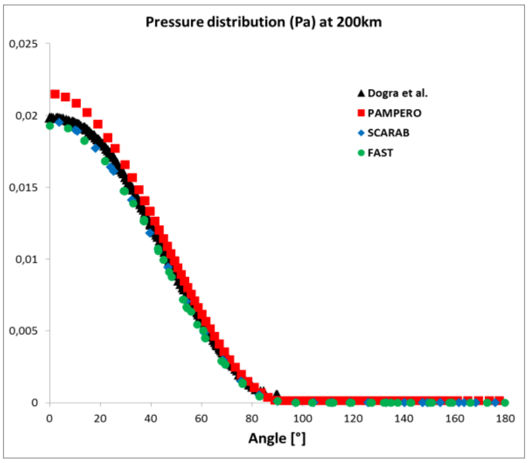

Figure 3: Pressure distribution at 90, 130 and 200 km

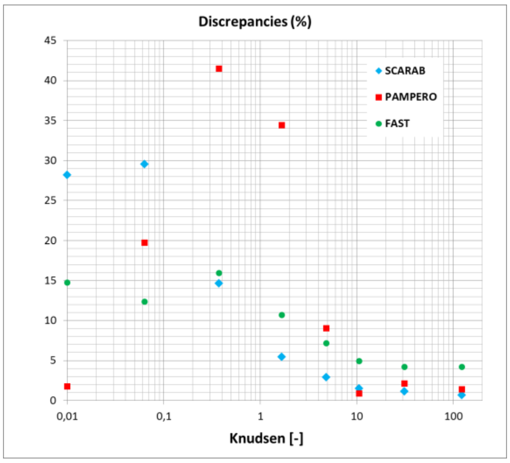

Figure 4: Stagnation point heat flux versus Knudsen number.

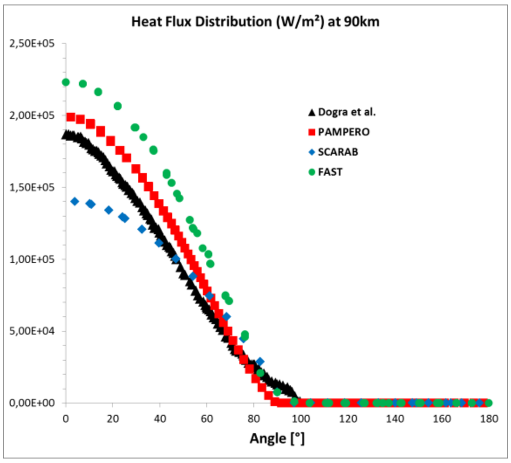

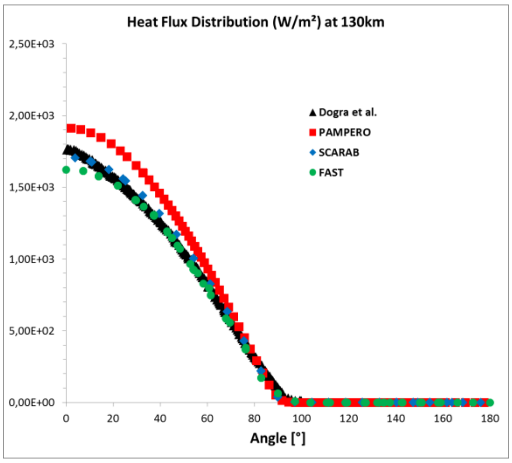

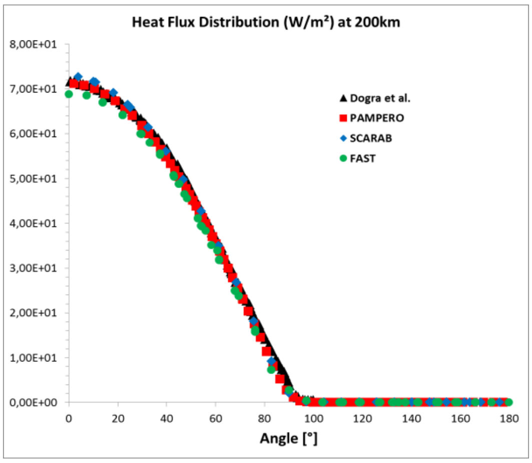

Figure 5: Heat flux distribution at 90, 130 and 200 km

3.2 The continuum regime – Simple geometries

Three kinds of geometry have been selected:

- The flat plate (infinite curvature radius issues)
- The tube (shock-shock interaction issues)
- The hollow sphere (concave surface issues)

Geometrical dimension are summarized in Table 2.

	Tube	Hollow Sphere	Plate
Diameter/Width [m]	1	4	3
Length [m]	1		1
Thickness [m]	0.25	0.1	0.1
AoA [°]	0	0	0

Table 2: Geometrical dimension

In the present study one angle of attack α has been studied. Each comparison is performed in wind-tunnel configuration. Only one trajectory point is retained for all objects. Upstream conditions are defined in Table 3.

Mach [-]	15
Velocity [m/s]	4769.73
Altitude [km]	58
Temperature [K]	250.61
Pressure [Pa]	26.3
Density [kg/m^3]	3.64 10^{-4}
Re/m [m^{-1}]	98573.316
Wall temperature [K]	700

Table 3: Upstream conditions

Results from PAMPERO, SCARAB, FAST/MUSIC are also compared to CFD in order to verify their accuracy. CFD computations were realized using the fluid dynamic code MISTRAL. Calculations are performed in continuous flow mode, with laminar assumption. Real gas effects and chemical reactions are also taken into account.

i) Flat plate

Figure 6 presents the drag coefficient and the integrated heat flux for the plate for the upstream conditions in Table 3. Moreover, Figure 7 presents different slices on the plate, where the pressure and heat flux distributions are plotted, in order to identify and understand possible discrepancies between spacecraft-oriented tools and CFD computations.

A very good agreement is noticed for the drag coefficient from all the spacecraft-oriented tools with MISTRAL. The pressure distribution on the main part of the front face is well estimated by PAMPERO, SCARAB and FAST/MUSIC. Some discrepancies arise close to the trailing edges, phenomena not predicted by such tools due to the modified Newton law assumptions. The pressure distribution on the side surface cannot be estimated by PAMPERO, SCARAB, FAST/MUSIC (considered as hidden surface) but MISTRAL confirms that its influence is negligible.

An important under-estimation from PAMPERO & FAST /MUSIC (resp. 68 % & 54%) on the integrated heat flux is noticed, explained by the non-negligible influence from the side faces considered hidden by such tools. An important over-estimation from SCARAB (105%) on the integrated heat flux is also observed. The side faces are described with uniform profile face whereas MISTRAL exhibits a decreasing profile.

The contribution from the back surface is negligible for this geometry.

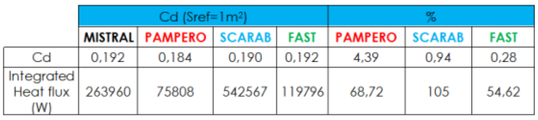

	Cd (Sref=1m²)				%		
	MISTRAL	PAMPERO	SCARAB	FAST	PAMPERO	SCARAB	FAST
Cd	0,192	0,184	0,190	0,192	4,39	0,94	0,28
Integrated Heat flux (W)	263960	75808	542567	119796	68,72	105	54,62

Figure 6: Drag coefficient and integrated heat flux for the plate

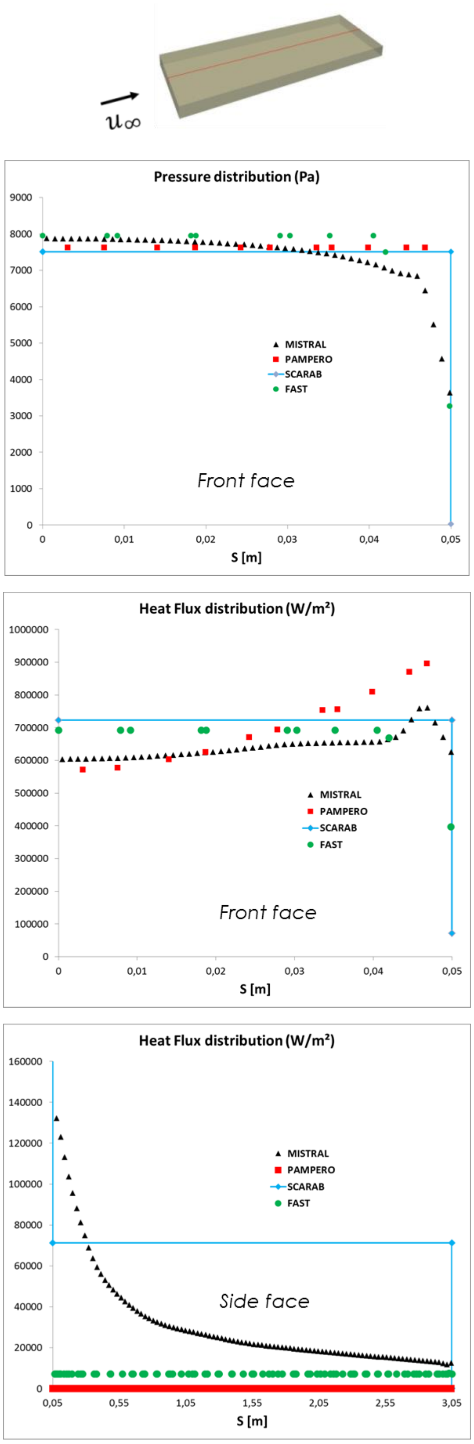

Figure 7: Pressure and heat flux distribution along the plate

ii) Tube

Figure 8 presents the drag coefficient and the integrated heat flux for the tube for the upstream conditions in Table 3. Moreover, Figure 9 presents different slices on the plate, where the pressure and heat flux distribution is plotted. The drag coefficient is not available with SCARAB for this object.

Notable differences (around 27%) are foreseen between PAMPERO & FAST/MUSIC with MISTRAL on the drag coefficient. Pressure and heat flux distributions are well estimated on the front face except on trailing edges where elliptic phenomena are still important and cannot yet be predicted. The contribution from the inner face is important for pressure and heat flux estimation (shock-shock interaction phenomena), but considered hidden for all spacecraft-oriented tools. This explains why the agreement is not perfect (from 47 to 66% for the integrated heat flux). Indeed, the inner surface contribution for the integrated heat flux has been calculated by CFD solutions and is equal to 35% of the total integrated heat flux. The contribution from the back face is negligible for this geometry.

	Cd (Sref=1m^2)				%		
	MISTRAL	PAMPERO	SCARAB	FAST	PAMPERO	SCARAB	FAST
Cd	1,528	1,082		1,128	29,20		26,16
Integrated Heat flux (W)	644958	220022	339454	271989	65,89	47,37	57,83

Figure 8:.Drag coefficient and integrated heat flux for the tube

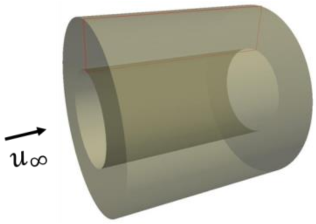

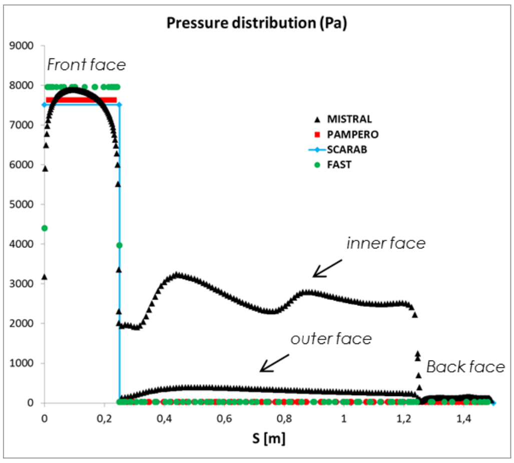

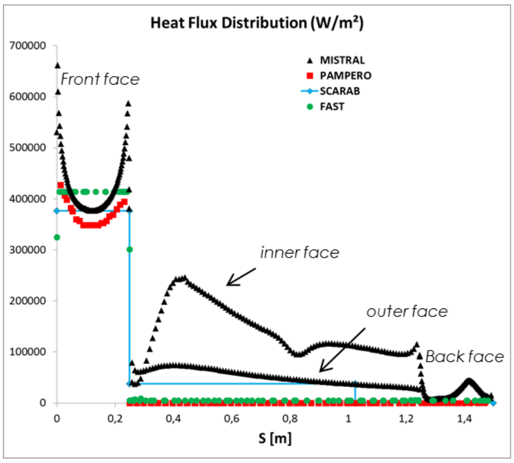

Figure 9: Pressure and heat flux distribution along the tube

iii) Hollow sphere

Figure 10 presents the drag coefficient and the integrated heat flux for the hollow sphere for the upstream conditions in Table 3. Moreover, Figure 11 presents different slices on the plate, where the pressure and heat flux distribution is plotted. The drag coefficient and the integrated heat flux are not available with SCARAB for this object.

Noticeable differences occur for PAMPERO (43%) and FAST/MUSIC (32%) for the drag coefficient and for the integrated heat flux (respectively 27% and 35%). Indeed, modified Newton law assumption is not appropriate for the spherical concave objects. Consequently, extrapolation function to assess the heat flux distribution along the concave sphere is also not appropriate. The contribution from the back sphere is negligible

	Cd (Sref=1m^2)				%		
	MISTRAL	PAMPERO	SCARAB	FAST	PAMPERO	SCARAB	FAST
Cd	22,20	12,66		15,06	43,24		32,16
Integrated Heat flux (MW)	2,50	3,18		3,38	27,12		35,51

Figure 10: Drag coefficient and Integrated heat flux for the hollow sphere

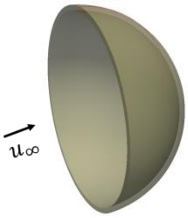

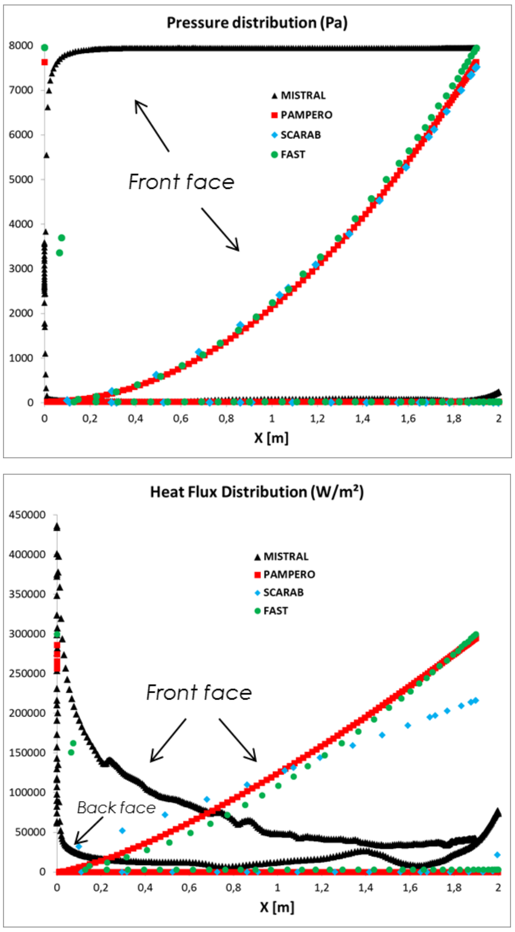

Figure 11: Pressure and heat flux distribution along the hollow sphere

3.3 The continuum regime – Space vehicles

Spacecraft designing strategy begins with help of pre-design tools to optimize geometrical configurations and trajectories regarding aerothermodynamic loads. This initial phase of selection is necessary before the intensive use of CFD solutions/experiments to develop pre-flight Aerodynamic/Aerothermodynamic databases. Following test cases based on ARD (flight realized in 1998) and Pre-X (CNES initial version of ESA IXV that flew in 2015) amid several other atmospheric re-entry vehicles aim at extending above debris-like critical analysis to classical controlled flying vehicles.

i) ARD case

The ARD has an axisymmetric Apollo-like shape composed of a spherical capsule following by a tore and a conical surface (Figure 12). It has an external diameter of 2.80 m, a total length of 2.04 m and an initial mass of 2753 kg. The nose radius is equal to the radius of the spherical part facing to the flow, so $R_n = 3.36\ m$.

Two numerical computations have been realized with MISTRAL [6] and LORE [9] CFD codes for the flight point at $M_\infty = 24$, with an angle of attack (α) of 20° and no side slip angle ($\beta = 0°$). This flight point corresponds to the peak heating. Laminar Navier-Stokes simulations have been computed in chemical non-equilibrium (chemical kinetics model of Dunn-Kang). The wall is supposed fully catalytic. The wall temperature is fixed to 1500 K. The freestream conditions used for the computations are summarized in Table 4.

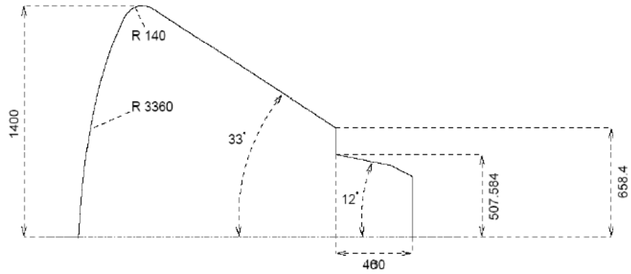

Figure 12. ARD geometrical configuration [9]. Dimensions are given in mm.

	ARD	Pre-X
Mach [-]	24	25
Altitude [km]	65.83	73.6
Velocity [m/s]	7212,43	7205
Density [kg/m^3]	1.5869 x 10^{-4}	5.546 x 10^{-5}
Temperature [K]	224.5	207
Pressure [Pa]	10.23	3.11
Wall temperature [K]	1500	1500
AoA [°]	20	40

Table 4. Freestream conditions used for computations in the both cases of ARD and PRE-X.

The stagnation point pressure coefficient and heat flux obtained with the CFD codes (MISTRAL, LORE) and the spacecraft-oriented tools (PAMPERO, FAST/MUSIC) are compared in Table 5. The results along the symmetry plan $y = 0\ m$ are drawn in Figure 13.

The stagnation pressure coefficient is successfully predicted by PAMPERO and FAST/MUSIC since a maximum difference of 5.1% and 0.5% with CFD data (MISTRAL or LORE) is noticed respectively.

A good consistency is observed between MISTRAL, LORE and flight data for the pressure coefficient distribution along the symmetry plan $y = 0\ m$. Although FAST/MUSIC over-estimates the pressure coefficient and PAMPERO under-estimates it, the obtained values are included into the error bars associated to the flight data.

Code	Cp [-]	Q [kW/m²]
MISTRAL	1.93	595
LORE	1.94	539.2
PAMPERO	1.84	528.3
FAST	1.94	537.8

Table 5. Comparison of stagnation pressure coefficient and heat flux obtained with CFD codes (MISTRAL, LORE) and Spacecraft-oriented codes (PAMPERO, FAST/MUSIC) in the case of ARD.

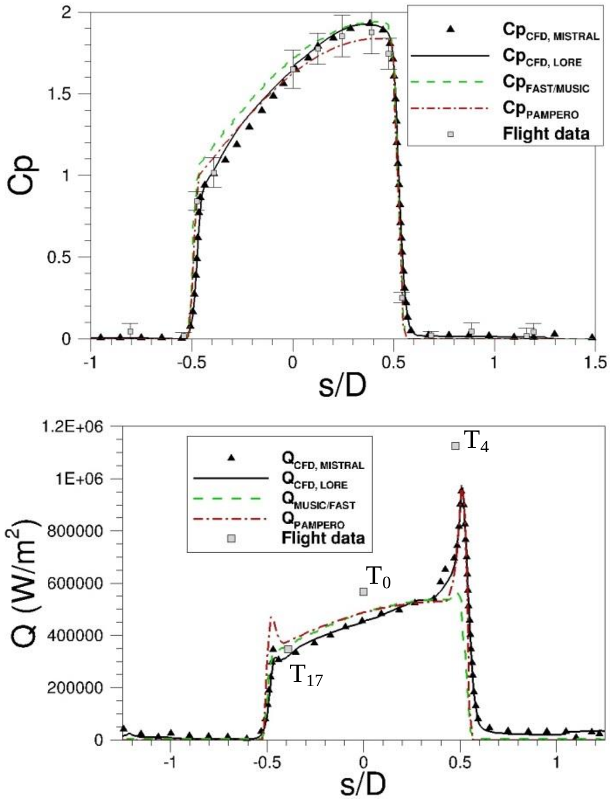

Figure 13. Comparison of pressure coefficient and heat flux obtained with CFD codes (MISTRAL, LORE), Spacecraft-oriented codes (PAMPERO, FAST/MUSIC) with flight data [10] along the symmetry plan (y = 0 m) of ARD.

The stagnation point heat flux seems to be correctly predicted by PAMPERO and FAST/MUSIC regarding to LORE-MISTRAL result, since a difference of 2%-11.2% and 0.26%-9.6% is recorded respectively.

Flight heating rate have been computed by [10] from temperature evolution versus time during the re-entry given by thermocouples implemented into the wall material. According to [10], thermocouples responses were satisfactory for $T \lesssim 973\,K - 1073\,K$. When T is above to these values, unexpected temperature evolution is then recorded leading to difficult measure conditions encountered during the entry. Therefore, the flight total heat flux on the front-shield is uncertain. The surface catalysis process begins at 77 km for a Mach number $M_\infty = 26$, while the peak heating is recorded at 65 km with $M_\infty = 24$.

The maximum heat flux is not located at stagnation point (stagnation pressure) but just ahead of the trailing edge of the capsule due to 21° angle of attack. Indeed, the flow acceleration induces a boundary layer thinning and thus an increase of the temperature gradient and finally the over-heating (Figure 14).

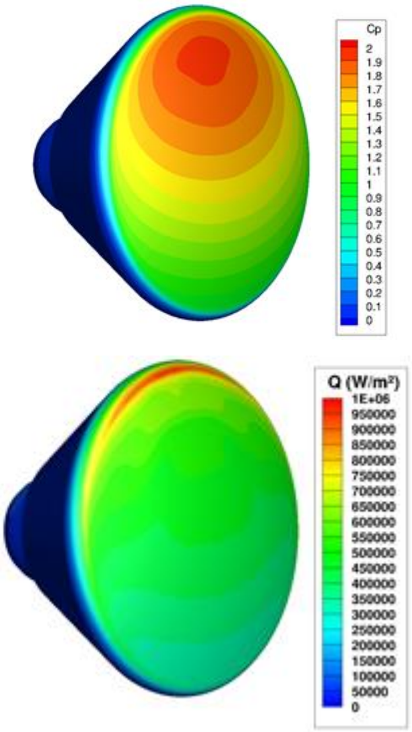

Figure 14. MISTRAL pressure coefficient and total heat flux distribution on ARD capsule.

The maximum heat flux recorded is about 1.2 MW/m^2 at T_4 thermocouple location (Figure 13). As quoted by [10], the amplification factor between T_0 and T_4 is about 2, which is significantly higher than predicted by MISTRAL and LORE. It makes some wondering about the level of accuracy we can expect for thermocouple measurement at heatshield shoulder. In the same way, under-meshing strategy in this region for CFD can also induce a quite weak capture of the real temperature gradient. Finally, heat flux distribution is correctly predicted by both PAMPERO and FAST/MUSIC compared to CFD results except at the trailing edges. Indeed, at $\frac{s}{D} \sim +0.5$, FAST/MUSIC under-estimates the heat flux by 51% (against 0.62% for PAMPERO), while PAMPERO over-estimates the heat flux by 35% (against 4% for FAST/MUSIC) at $s/D \sim -0.5$.

ii) PRE-X case

The primary objective of the PRE-X vehicle project was to obtain flight data in order to improve thermal protection system and aerothermodynamics knowledge for future European reusable vehicle. This project started in 2000 has been stopped in 2007 and replaced by ESA IXV Program then flew successfully by beginning 2015. The PRE-X had a length without flaps of 4 m and a reference surface of 6 m². The nose radius is equal to 0.925 m.

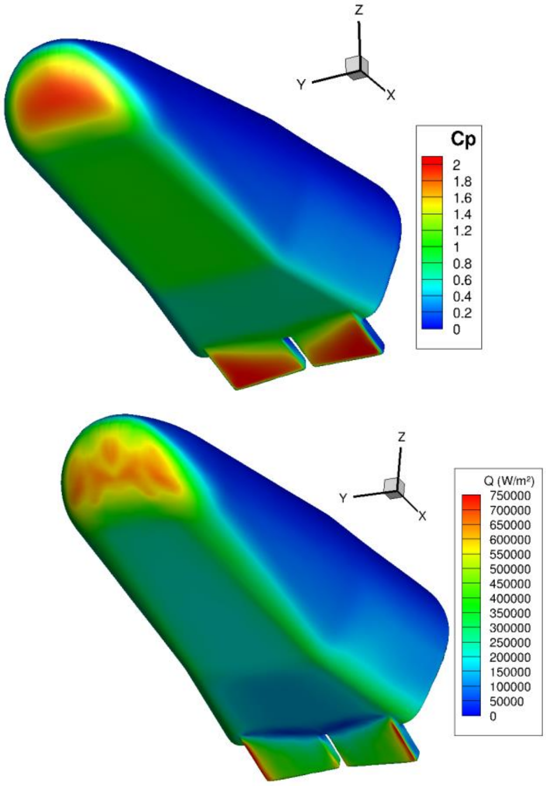

Figure 15. CELHYO pressure coefficient and total heat flux distribution on PRE-X.

Two numerical computations have been realized with MISTRAL [6] and CELHYO [11] CFD codes for the flight point at $M_\infty = 25$, with an angle of attack (α) of 40° and no side slip angle ($\beta = 0°$). Laminar Navier-Stokes simulations have been computed in chemical non-equilibrium. The wall is supposed fully catalytic. The wall temperature is fixed to 1500 K. The freestream conditions used for the computations are summarized in Table 4.

The stagnation point pressure coefficient and heat flux obtained with the CFD codes (MISTRAL, CELHYO) and both spacecraft-oriented tools (PAMPERO, FAST/MUSIC) are compared in Table 6.

Code	Cp [-]	Q [kW/m²]
MISTRAL	1.91	593
CELHYO	1.91	588
PAMPERO	1.83	557
FAST	1.94	603

Table 6. Comparison of stagnation pressure coefficient and heat flux obtained with CFD codes (MISTRAL, CELHYO) and Spacecraft-oriented codes (PAMPERO, FAST/MUSIC) in the case of PRE-X.

The stagnation pressure coefficient is successfully predicted by PAMPERO and FAST/MUSIC since a difference of 4.2% and 1.5% with CFD data (CELHYO and MISTRAL) is observed respectively. Moreover, the stagnation point heat flux seems to be correctly predicted by PAMPERO and FAST/MUSIC regarding to both CFD CELHYO and MISTRAL results, since a difference of 5.3%-6.1% and 2.6%-1.7% is recorded respectively.

The results along the plan $y = 0\,m$ and $y = 0.3\,m$ are plotted in Figure 16 and Figure 17 respectively. Five zones are identified:

- Zone 1 ($x \in [0\,m; 0.7\,m]$) corresponds to the stagnation point area. The pressure distribution computed by the modified Newtonian method (PAMPERO and FAST/MUSIC) is similar to the CFD results. The heat flux computed by the Spacecraft-oriented codes is also well predicted. However, a mesh related problem has induced an unusual peak heat flux for PAMPERO in this area.
- Zone 2 ($x \in [0.7\,m; 2.5\,m]$) corresponds to the first flat surface. The pressure distribution is lightly under-estimated by PAMPERO (9.2%) and FAST/MUSIC (4.1%) in comparison to CELHYO and MISTRAL. The constant pressure assumption is valid since the shock layer around the PRE-X is quite thin. The heat flux computed by the Spacecraft-oriented codes is also well predicted in this area with a relative difference of between 0.6% and 8% (PAMPERO) and between 2.6% and 27% (FAST/MUSIC) regarding to CFD results.
- Zone 3 ($x \in [2.5\,m; 3\,m]$) corresponds to the transition between the primary and the secondary flat surface. This slope break induces a slight pressure decrease which is correctly predicted by PAMPERO and FAST/MUSIC. While the heat flux computed by CFD tools also decreases, an unphysical peak heat flux is calculated by PAMERO and FAST/MUSIC. The dependence of the heat flux distribution model to the local curvature radius causes this wrong level.

- Zone 4 ($x \in [3\,m; 3.6\,m]$) corresponds to the secondary flat surface. The pressure and heat flux in this area are smaller than in zone #2 due to the flow expansion in zone #3. A mean difference of 11.3% and 17.7% with CFD results is obtained by PAMPERO and FAST/MUSIC respectively for the pressure distribution. The discrepancy is around 20.3% (PAMPERO) and 1.3% (FAST/MUSIC) for the heat flux.
- Zone 5 ($x \in [3.6\,m; 4\,m]$) corresponds to the recirculation area located upstream of the flaps (with a deflection angle δ of 15°). This zone is characterized by a pressure increase and a heat flux decrease. These are induced by a flow compression due to the presence of the flaps. The analytical models implemented in PAMPERO and FAST/MUSIC cannot predict this phenomenon.
- Zone 6 ($x \in [4\,m; 4.4\,m]$) corresponds to the flaps location (Figure 17 only). Here, the pressure and heat flux peak recorded is induced by the flow topology (flow detachment – reattachment). Once again, the analytical model cannot predict these phenomena.

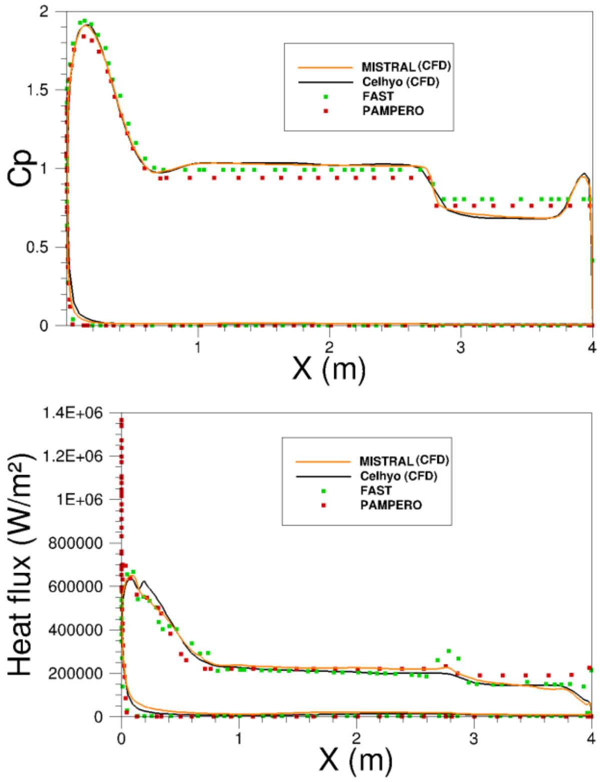

Figure 16. Comparison of pressure coefficient and heat flux obtained with CFD codes (MISTRAL, CELHYO and, Spacecraft-oriented codes (PAMPERO, FAST/MUSIC) along the symmetry plan (y = 0 m) of PRE-X.

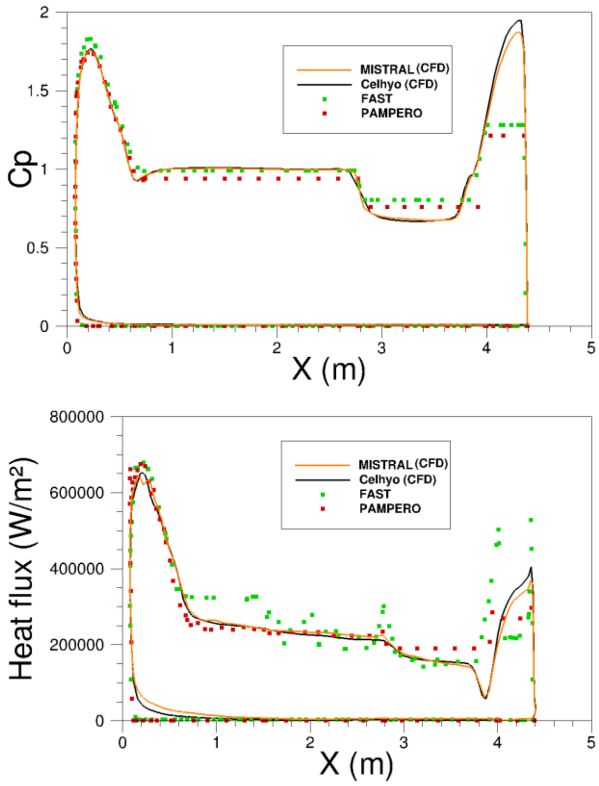

Figure 17. Comparison of pressure coefficient and heat flux obtained with CFD codes (MISTRAL, CELHYO and, Spacecraft-oriented codes (PAMPERO, FAST/MUSIC) along the plan (y = 0.3 m) of PRE-X.

4 CONCLUSIONS

Spacecraft-oriented codes have been compared to numerical results and flight data in terms of pressure coefficients and heat flux. Limits of the Newtonian method to compute the pressure distribution are well known in the literature. Moreover, the comparison of Spacecraft-Oriented codes heat flux models with numerical results or flight data has shown the limitation of these models. So, one of the future developments of these codes concerns the addition of a model allowing to determine the pressure and heat flux value in presence of recirculation and flow expansion zone.

For way of improvements, we propose to:

- Calibrate/refine bridging function for the transitional regime with DSMC and/or Navier-Stokes (continuum boundary) codes
- Deal with hidden surface (e.g. side face for the plate, inner face of the tube, back faces)
- Deal with shock-shock interaction phenomena (e.g. inner face of the tube)
- Deal with trailing edge elliptic phenomena
- Deal with concave surfaces

5 REFERENCES

1. J. Annaloro, S. Galera, P. Kärräng, G. Prigent, T. Lips, P. Omaly (2017) *Comparison between two spacecraft-oriented tools: PAMPERO & SCARAB* The Journal of Space Safety Engineering, http://dx.doi.org/10.1016/j.jsse.2017.02.004

2. P. Omaly, M. Spel, (2012) *DEBRISK, a tool for re-entry risk analysis.* Proceedings of the 5th IAASS Conference A Safer Space for Safer World. Noordwijk, Netherlands

3. J. Annaloro, P. Omaly, V. Rivola, M. Spel (2014) *ELABORATION OF A NEW SPACECRAFT-ORIENTED TOOL: PAMPERO,* 8th European Symposium on Aerothermodynamics for Space Vehicles, Lisbon

4. T. Lips *et al.*, *RE-ENTRY RISK ASSESSMENT FOR LAUNCHERS – DEVELOPMENT OF THE NEW SCARAB 3.1L*, 2nd IAASS Conference, Chicago, USA, May 14–16, 2007

5. Y. Prévereaud, J.-L. Vérant, M. Balat-Pichelin, J.-M. Moschetta, *(2015) Numerical and experimental study of the thermal degradation process during the atmospheric re-entry of a TiAl6V4 tank.* Acta Astronautica, Vol. 122, pp. 258-286.

6. T. Scott, W. Dieudonné, M. Spel, MISTRAL: CONUS Debut Flow Field and Heat Transfer Calculations, 34th AIAA Fluid Dynamics Conference and Exhibit, Portland, 2004

7. Jouhaud, F. (2011). Mécanique du Vol Atmosphérique et Spatial : Recueil de modélisations, Rapport Technique NT4/17163 DCSD, ONERA

8. Sippel, M., Bussler, L., Kopp, A., Krummen, S., Valluchi, C., Wilken, J., Prévereaud, Y., Vérant, J-L., Laroche, E., Sourgen, F., Bonetti, D. (2017). *Advanced Simulation of Reusable Hypersonic Rocket-Powered Stages*, 21st AIAA International Space Planes and Hypersonic Systems and Technologies Conference AIAA 2017-2170, Xiamen, China.

9. V. K. Dogra, et al., *Aerothermodynamics of a 1.6-Meter-Diameter sphere in hypersonic rarefied Flow,* AIAA-91-0773, 29th Aerospace Sciences Meeting, 1991, 10.2514/6.1991-773.

10. Walpot, L. (2002). *Development and application of a hypersonic flow solver* (Ph.D thesis), Deft Technical University, The Netherlands.

11. Tran, P., Paulat, J.C., Boukhobza, P. (2007). *Re-entry flight experiments lessons learned – the atmospheric re-entry demonstrator ARD, Flight Experiments for Hypersonic Vehicle Development,* RTO-EN-AVT-130, pp.10-1–10-46.

12. Thivet, F., Hylkema, J., Spel, M., Dieudonné, W. (2005). *Detailed aerothermodynamical analysis of Pre-X*, 4th International Symposium Atmospheric Reentry Vehicles and Systems, Arcachon, France.